ROYAL SOCIETY OF CHEMISTRY

PAPER

Check for updates

Probing dynamic degradation and mass transport in solid-state sodium-ion batteries using operando simultaneous dual-polarity SIMS†

Sivakkumaran Sukumaran,*[a] Richard J. Chater,[a] Sarah Fearn,[a] Graham Cooke,[c] Noel Smith[d] and Stephen J. Skinner [iD] *[a,b]

Operando investigation of a solid-state battery is challenging due to sample conditions, such as electrode roughness and sensitivity to the atmosphere. In this work, we present an *operando* technique that combines electrochemistry with the simultaneous detection of secondary ions in a Hi-5 Secondary Ion Mass Spectrometer (SIMS). Sodium metal|NASICON solid electrolyte interfaces were formed through cycling at different current densities in a 1 μm^2 region, where the critical current density was found to be 0.04 μA μm^{-2}. Electrochemical Impedance Spectroscopy (EIS) determined that a solid electrolyte interphase (SEI), resistive to sodium-ion migration, formed at each sodium metal|NASICON interface. Dynamic dual-polarity SIMS identified the SEI to be composed of oxide species that formed along the sodium mass transport columns and degraded the grain boundaries, leading to dendrite formation at the sodium metal|NASICON interfaces. This work pioneers a new diagnostic tool, propelling interfacial and solid electrolyte engineering solutions to mitigate device failure, allowing the development of next-generation solid-state batteries.

Broader context

Investigating degradation mechanisms within solid-state batteries presents several challenges as the electrochemical changes of the battery are required to be correlated with structural changes under real-world operating conditions. Typically, the areas of interest within the battery, such as the solid-electrolyte interfaces and the solid-electrolyte itself, are reactive under ambient conditions, leading to processes taking place due to cell disassembly and transfer to analytical tools. These processes lead to difficulty in correlating the cell performance and degradation mechanism with the structural, microstructural and chemical evolution of the battery. Here we report an *operando* characterisation technique that will track the electrochemical degradation at the nanoscale of a solid-state battery under operating conditions, where *operando* regions of interest can be formed under ultra-high vacuum. This *operando* technique combines both electrochemistry and chemical analysis and is demonstrated on a solid-state sodium-ion battery (SSIB) using a sodium metal|NASICON anode interface model system. The powerful insights presented by the technique are a step forward in advancing battery science and can be applied as an investigative or diagnostic tool for solid-state batteries. More importantly, we envisage that this technique can be widely applied to obtain a fundamental understanding of mass transport and degradation mechanisms in faradaic-based systems.

Introduction

Solid-state sodium-ion batteries (SIBs) have gained global interest as an alternative energy storage device for grid-storage and low-end vehicles. This is due to abundant resources, no geopolitical constraints, and low material cost when compared to lithium-ion batteries. For emerging economies that require an affordable energy storage device to supplement growth, SIBs offer a viable solution.[1,2] Conventional SIBs are constructed using a solid electrolyte and are safer compared to lithium-ion batteries (LIBs) that use aqueous solutions. To provide comparable energy and power density to LIBs, SIBs use sodium metal as the anode.[3] Considerable interest has been shown in developing alternative anode materials for SIBs;[3] however, in order to expand their commercial viability, further advances in solid electrolytes are required as they facilitate the migration of charge carriers to and from the electrodes. Various solid electrolytes can be utilised in SIBs, with the most prominent being the sodium super-ionic conductor (NASICON).[4,5]

NASICON-based solid electrolytes allow the scalability of SIBs due to their low cost of manufacturing and high ionic

[a]*Imperial College London, Department of Materials, Exhibition Road, London, SW7 2AZ, UK. E-mail: s.sukumaran20@imperial.ac.uk*

[b]*International Institute for Carbon Neutral Energy Research, Kyushu University, 744 Motooka, Nishi-ku, Fukuoka 819-0395, Japan*

[c]*Hiden Analytical, 420 Europa Blvd., Warrington, WA5 7UN, UK*

[d]*Oregon Physics, Greenbrier Parkway, Beaverton, OR 97006, USA*

conductivity at ambient temperature, and the incorporation of dopants allows further improvements.[6,7] Although NASICON is a promising solid electrolyte, the electrochemical stability at the alkali metal anode|solid electrolyte interface needs to be investigated. The interface is the immediate point of contact between the solid electrolyte and the anode, promoting the electrochemical processes that facilitate the operation of the battery. Consequently, any mechanistic and chemical changes at the interface, *e.g.* solid electrolyte interphase (SEI) formation, will have a profound impact on the functionality of the device.

In current studies,[8–12] the chemical instability of the sodium metal|NASICON interface has been reported, as NASICON is thermodynamically unstable against sodium. Through direct contact or sodium mass transport (sodiation), the following reaction products are formed: Na_2ZrO_3, Na_4SiO_4, Na_3P and ZrSi. The combination of these products can be attributed to an SEI and acts as a passivation layer that is electronically insulating but ionically conductive. The impact of the SEI and its exact location on the interface or sodiation has not been fully investigated. Building upon previous work[13] on *in situ* characterisation of the alkali metal anode|solid electrolyte interface using secondary ion mass spectrometry (SIMS) to determine SEI formation, an *operando* technique has been developed to determine the SEIs' role in the performance and durability of SIBs, where a specific electrochemical load can be applied across the solid electrolyte in a controlled process to form SEIs. Tolerance under load or failure can then be diagnosed to obtain mechanistic and chemical understanding that can be used to engineer solutions for next-generation SIBs.

In this work, a sodium-ion solid-state half-cell using NASICON with the stoichiometry of $Na_{3.4}Zr_2Si_{2.4}P_{0.6}O_{12}$ was investigated *operando* using the Hi-5 SIMS instrument. Specific current densities were applied across the surface of the NASICON to cause sodiation, resulting in the nucleation of sodium metal at the surface – forming *operando* sodium metal|NASICON interfaces. Cycle graphs were recorded during sodiation and indicated the voltage response of the cell, which was attributed to cycled or failed regions, and a critical current density (CCD) was determined. Electrochemical Impedance Spectroscopy (EIS) was used to identify the components that facilitated sodiation to form the interfaces and were found to fit equivalent circuit models. The sodiated regions, including the SEI, were then analysed through dynamic dual-polarity SIMS analysis to chemically identify sodiation and composition. The mechanisms behind SEI formation and sodiation were determined, and it was found that sodium formed transport columns that propagated through the bulk and grain boundaries. Along and around these transport columns, electrochemical degradation was observed with the primary fragments being ZrO_2, SiO_2, and PO_2, which can be attributed to the decomposition products Na_2ZrO_3, Na_2SiO_3 and Na_3P, confirming that the SEI is not self-limited. This work corroborates the findings to date on the electrochemical stability of NASICON in sodium-ion batteries and crucially allows *operando* characterisation for SIBs, allowing mechanistic and

chemical understanding of mass transport and electrochemical degradation in solid-state batteries.

Results and discussion

### *Operando* cycling of a solid-state sodium-ion half-cell

To mimic an SIB mode of operation, a solid-state half-cell was mounted as shown in Fig. 1a. Through the probes, a constant current was supplied to generate an electric field that could be applied to specific regions across the NASICON surface to generate a potential difference (Fig. 1d). Sodium ions (Na^+) diffused through the NASICON from the sodium metal electrode (on the underside of the cell), towards areas where the probes are positioned (Fig. 1b).

To confirm that sodiation has occurred, one of the islands formed across the NASICON surface was analysed by simultaenous[14] dual-polarity SIMS (Fig. 1c). From the elemental ion maps, the difference in concentration between Na, Zr, Si and P, in areas where sodiation has occurred, validate that the islands formed are composed of sodium metal originating from the positive electrode. This is also confirmed by the O ion map, which highlights the area in which sodium has nucleated. After sodiation, a passivation reaction composed of NaO forms, this increases the wettability between sodium metal and NASICON, leading to enhancement in the O signal.[15] The islands suggest that as sodium approaches the surface, the electric field around the probe (Fig. 1d) causes the sodium to nucleate. As the electric field is directly proportional to the current density, when it expands so to do the sodium islands (Fig. 1b). In Fig. 1b(v), the sodium island spans over a large area approx. 112 μm × 112 μm, when compared to Fig. 1b(ii) where the area is approx. 20 μm × 20 μm. The difference in current density applied offers a visual indication of the mechanism of sodiation. When applying current densities that the solid electrolyte can tolerate, 'homogenous' plating occurs, where 'well-rounded' islands are localised to the electric field form (Fig. 1b(i)). If the current density applied is greater than the critical current density (CCD) – the maximum current density that the solid electrolyte can tolerate before failure, then 'inhomogeneous' plating occurs, indicated by the irregular shape of the sodium island in Fig. 1b(v). This suggests that a sodium dendrite has formed, as the sodium has nucleated in regions that are extended from the probe (placed on the left-hand side of the island in Fig. 1b(v)). This implies that specific regions across the NASICON can be cycled at a specific current density, by repeatedly applying a constant current, where a CCD can be determined, or failed. Thus, the alkali metal anode|solid electrolyte interface, including any chemical changes *e.g.* a SEI, and failure mechanism can be investigated.

Sodium dendrite formation and grain boundary degradation

Regions across the NASICON surface were sodiated with increasing current densities, and a cycle graph was obtained to indicate whether the region can be cycled or failed. Cycled regions can be defined as little to no offset, which represents
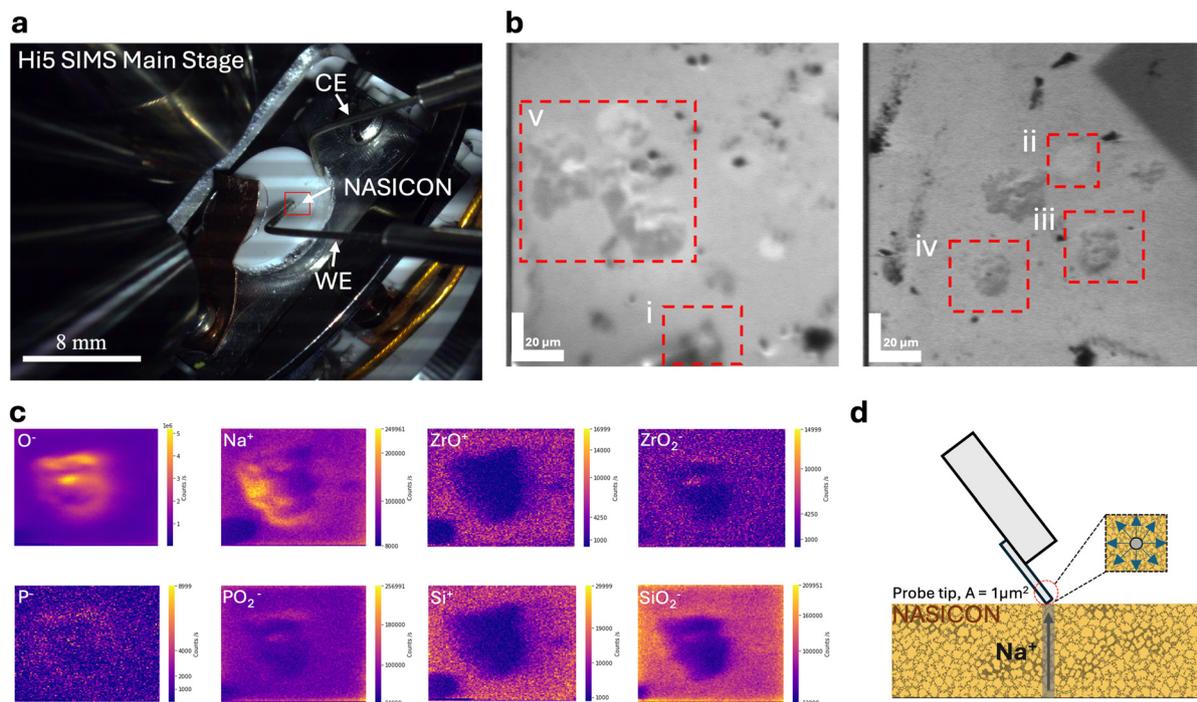
Fig. 1 Operando nucleation of sodium across a NASICON surface. (a) Optical image of the Hi5 SIMS main stage with the sodium-ion solid-state half-cell with Kliendiek probes acting as working electrode (WE) and counter electrode (CE) connections. The red square with arbitrary dimensions is used for guidance to highlight the area where the beam can be applied. (b) Secondary electron images of sodium islands at different current densities (highlighted in the red box) (i) 0.02 $\mu A\ \mu m^{-2}$, (ii) SEI formed with 0.04 $\mu A\ \mu m^{-2}$, (iii) 0.1 $\mu A\ \mu m^{-2}$, (iv) 0.2 $\mu A\ \mu m^{-2}$, (v) 0.5 $\mu A\ \mu m^{-2}$. (c) Dual-polarity elemental ion maps, collected simultaneously, of the sodium island produced with a current of 0.02 $\mu A\ \mu m^{-2}$. (d) Schematic of the driving force behind nucleation of sodium islands at the NASICON surface, where Na^+ represents the sodium metal; the inset shows an approximation of the electric field of the probes upon contact with the surface.

resistance, being present between the voltage and the current profile, whereas for a failed region a large offset is seen. Failure of a region can also be determined by a drop in the voltage response, that stabilises to half or lower than its original value. Cycle graphs of a cycled and failed region, recorded during sodiation inside the vacuum chamber, are shown in Fig. 2 with additional cycle graphs presented in Fig. S1.†

Through cycling with increasing current densities at different regions, the maximum CCD of NASICON was determined to be 0.04 $\mu A\ \mu m^{-2}$. This was indicated by both the voltage and current profile being in tandem with no significant offset (Fig. 2a). Although there is a disparity between the height of the current and voltage profile, this can be attributed to experimental artefacts. As the current is applied in a 1 μm^2 area, any surface inhomogeneity between the probe tip and surface can result in poor contacts, such as monolayers. The CCD was also determined by comparison with cycle graphs in Fig. 2a(ii) and Fig. S1(ii–iv),† where regions failed at 0.06 $\mu A\ \mu m^{-2}$, 0.1 $\mu A\ \mu m^{-2}$, 0.2 $\mu A\ \mu m^{-2}$, and 0.5 $\mu A\ \mu m^{-2}$, as a large offset between the voltage and current profile is seen. This suggests that at all of these failed regions, where only minor migration of sodium is allowed, a sodium dendrite has formed.

To assess cyclability at the CCD, the sodium island formed at a current density of 0.04 $\mu A\ \mu m^{-2}$ was cycled for one iter-

ation, with the cycle graphs recorded for each process (stripping and plating) shown in Fig. 2b. In the stripping process (Fig. 2b(i)), where sodium in the island is driven towards the positive electrode, the voltage response gradually increases as the reservoir of sodium depletes, until it spikes to around 13 V indicating depletion. The stripping process lasted approximately 0.6 min (40 s), which suggests that the migration of sodium is rapid and could be explained by the initial plating process establishing preferential transport pathways that control the migration process (Fig. 2a(i)). The region was then replated (Fig. 2b(ii)) and the voltage profile exhibits a similar pattern as seen in Fig. 2a, and differences can be seen. The voltage oscillations are less frequent, which suggests that the sodium is plated gradually due to the preferential transport pathways. Between 0 min and 3 min, a step-like feature is observed, which indicates that an electrochemical change has taken place. The region is now resistive to the mobility of sodium, indicated by the drop in voltage response, where originally it was oscillating between 40 mV to 60 mV, and has now stabilised to around ~40 mV. This would indicate that during cycling, decomposition products were formed to create an SEI that is resistive to sodium migration. If continuously cycled, the growth of this SEI would occur, leading to a region that is heavily resistive to sodium migration, and would contribute to dendrite formation. A dendrite forms as sodium diffuses
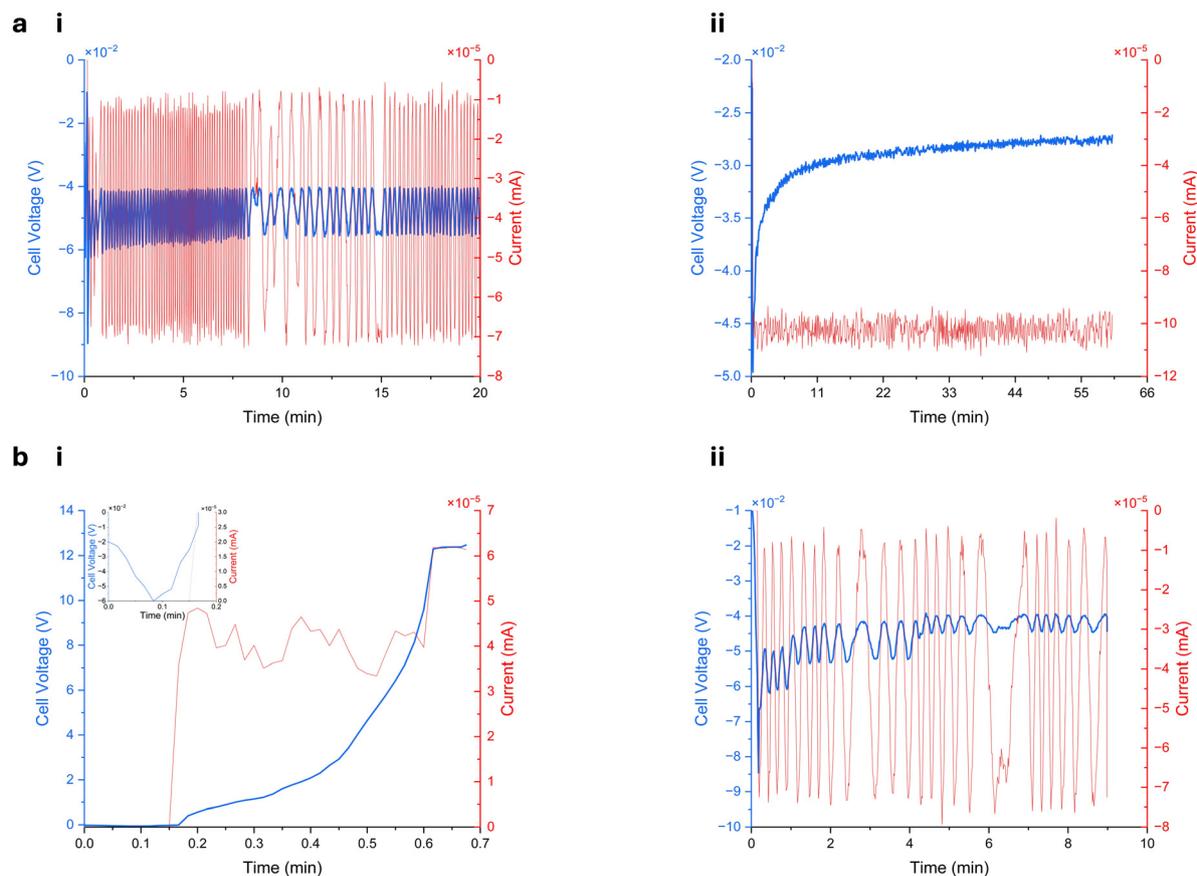
Fig. 2 Cycle graphs of sodiated regions. (a) Cycle graphs of sodium islands at different current densities (i) 0.04 μA μm^{-2} and (ii) 0.1 μA μm^{-2}. (b) Cycle graphs of a sodium island being cycled at 0.04 μA μm^{-2}; the left-hand side shows the cell response of stripping sodium and the right-hand side shows the cell response of re-plating sodium. The inset of b(i) shows voltage response below the origin.

through the SEI and towards the surface, and the ionic mobility is reduced leading to the likelihood of recombination with an electron, which would then cause sodium to isolate within the NASICON. The isolated sodium would continue to grow, forming a dendrite, until contact between the two electrodes has been made resulting in short-circuiting.

As migration of sodium is facilitated by both bulk and grain boundaries, impedance spectra were obtained at each island to assess any changes in these migration mechanisms and whether they can be correlated to an SEI or dendrite formation at cycled or failed regions. Spectra for the two distinct regions are shown in Fig. 3, and spectra for other islands are shown in Fig. S2.† The spectra were found to fit an equivalent circuit model, a resistor in parallel with a constant phase element (CPE). The components of the model can be attributed to a physical process, excluding bulk migration (as it requires a GHz frequency range[16]) and is instead represented by the offset from the origin (insets of Fig. 3a). The two parallel R-CPE circuit components have characteristic capacitances of grain boundary processes and an interfacial layer that was formed between the solid electrolyte and sodium island. The capacitance of the components was validated against the literature,[17] and these values along with other electrochemical para-

meters are presented in Table 1. Capacitance and electrochemical parameters calculated for the other islands are presented in Table S1.†

The spectrum of the cycled region at the CCD (Fig. 3a(i)), indicates that the grain boundary component becomes resistive. Although the increase in resistance is gradual, it indicates that as a function of sodiation, deterioration of the grain boundary migration occurs and is reflected by the decrease in grain boundary conductivity as the region is cycled at the CCD (Table 1). A similar increase in the resistance of the interfacial layer component should be observed in the second plating cycle at the CCD. However, the duration of the second plating cycle was half of the initial plating cycle. Thus, the sodium island that had formed encompassed a smaller area; therefore, the surface probed by EIS is smaller. Nonetheless, the spectrum indicates that a surface layer was formed during sodiation, which is more resistive than the grain boundary but allows sodium migration and can be attributed to an SEI. In comparison Fig. 3a(ii) shows the spectrum of a failed region, where the grain boundary and the SEI component is more resistive than the cycled region. Therefore, the failed region is more resistive to sodium migration and suggests that a dendrite is formed, as the grain boundaries and SEI now only
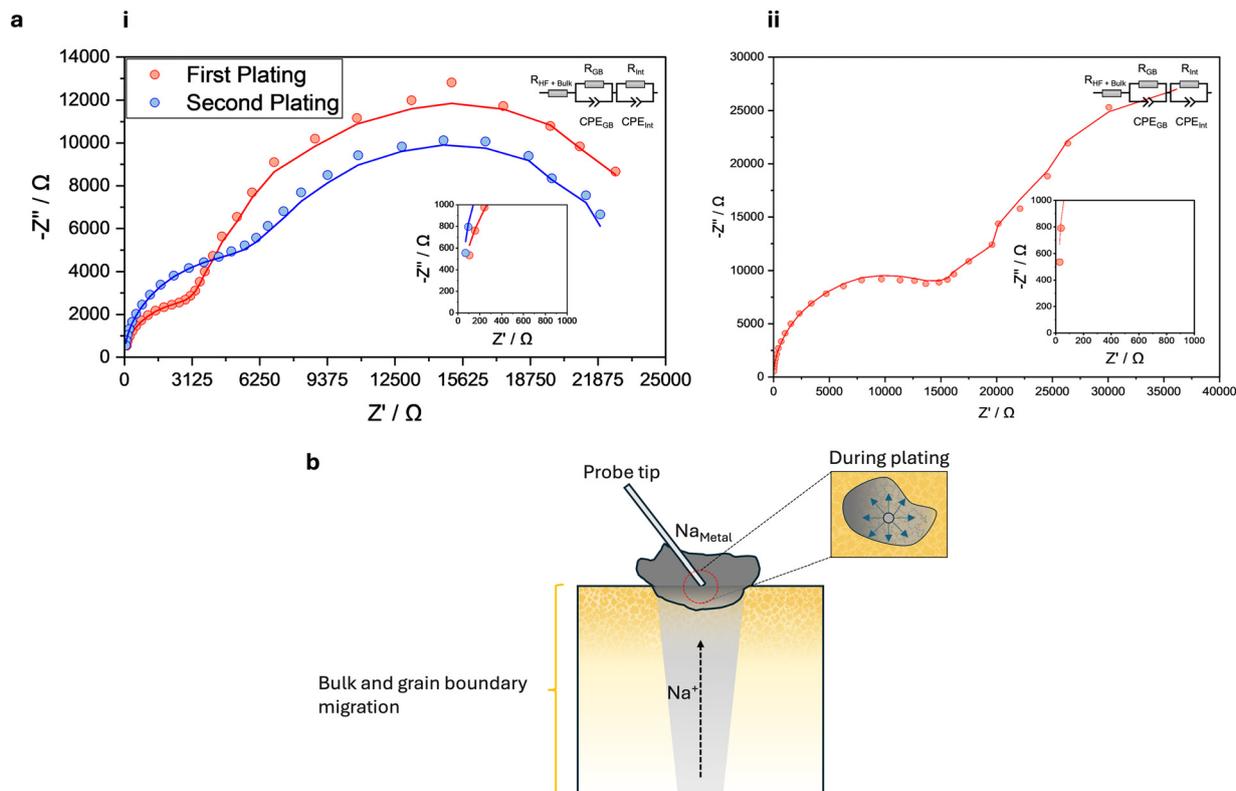
Fig. 3 Operando impedance spectra of sodiated regions. (a) Spectra obtained from each island (i) 0.04 μA μm^{-2} and (ii) 0.1 μA μm^{-2}, with the inset showing the offset from origin which indicates bulk response. Resistance of each component (Ω_{Gb} and Ω_{Int}) is measured in Ohms. (b) Schematic representation of migration mechanisms driving sodium to form islands at the surface, with the inset demonstrating the influence of the electric field on sodium as it approaches the surface.

Table 1 Electrochemical properties obtained from impedance fitting of sodiated regions

J (μA μm^{-2})	R_{Gb} (Ω)	R_{Int} (Ω)	C_{Gb} (10^{-10} F)	C_{Int} (10^{-9} F)	σ_{Gb} (10^{-1} S cm^{-1})
0.04 (I)	3188 (±204)	25 135 (±867)	3.1 (±0.9)	2.4 (±0.5)	4 (±0.4)
0.04 (II)	5993 (±547)	19 451 (±1148)	2.9 (±0.7)	1.6 (±0.6)	2.1 (±0.3)
0.1	15 794 (±907)	57 494 (±8979)	2.6 (±0.4)	3.6 (±2)	0.81 (±0.08)

Resistance, capacitance and grain boundary conductivity values of fitted semi-circles extracted from the Nyquist plots of the sodiated regions during *operando* measurement. Uncertainty was calculated by propagating the errors in the fitting and thickness of the pellet (±0.01 cm). Roman numeral beside 0.04 μA μm^{-2} indicates the plating cycle.

allow minor sodium migration which is indicated by the poor grain boundary conductivity (Table 1). This is further validated by the impedance spectra obtained for the other current densities (Fig. S2†). When comparing the spectrum obtained with the smallest current density (0.02 μA μm^{-2}) to current densities greater than the CCD, both grain boundary and SEI components become increasingly resistive which translates to poor grain boundary conductivity (Table S1†). It can be suggested that there is a relationship between the deterioration of grain boundary migration and SEI formation, as sodiation would not result in physical deterioration of the grain boundaries. Any deterioration would be electrochemical, which the SEI is a result of. Therefore, it can be implied that the SEI forms along

or in the vicinity of grain boundaries inhibiting sodium migration. This would explain the behaviour observed in the cycle graphs, where the voltage response diminished in the cycled region (Fig. 2b(i)) and a large offset is seen in the failed region (Fig. 2a(ii)). Thus, it can be demonstrated that regions across the solid-state sodium-ion half-cell can be cycled *operando*, and through cycle graphs and impedance spectra, the electrochemical behaviour of these regions can be monitored. Regions can be cycled at a CCD or failed through sodium dendrite formation. In both regions, SEI formation occurs and results in inhibiting grain boundary sodium migration. In regions where this SEI is present, dendrite formation is most likely to occur.

Simultaneous dual-polarity SIMS characterisation of the solid electrolyte interphase at sodiated regions

To chemically identify the SEI that led to degradation of the grain boundary migration and dendrite formation, depth profiles were taken in the sodium islands of the cycled and failed region (Fig. 4). A non-sodiated region was analysed to serve as a reference (Fig. 4(i)) and the chemical composition ratio of the surface to bulk region of NASICON was determined. The region is primarily composed of sodium, Na^+, and oxide species, SiO_2^- and PO_2^-, and towards the bulk Si^+, Zr^+, P^-, and Zr secondary species (ZrO^+ and ZrO_2^-) become prominent. Contributions to the ZrO_2^- concentration profile stem from the ZrO_2 secondary phase, due to sintering and synthesis at high temperature (see Methods), and are present at the surface to near-surface (0 μm–0.5 μm) and surface to bulk region (0 μm–2 μm), respectively. When sodiation occurs, changes in the chemical composition of the surface to bulk region are observed. From Fig. 4(ii), (iii) and Fig. S3,† a distinct chemical change can be seen from the increase in the ZrO^+ and ZrO_2^- profiles and can be associated to a decomposition reaction. In

profiles where current densities above the CCD were applied, ZrO_2^- appears to be concentrated in the bulk (Fig. 4(ii), S3(ii) and (iii)†). These observations suggest that the concentration of ZrO_2^- saturates around the sodium that is formed into a dendrite. For profiles where cycling has occurred or for the smallest current density applied (Fig. 4(ii) and Fig. S3(i)†), the increase in ZrO_2^- is gradual as the bulk is approached. This further suggests that there is a correlation between the ZrO_2^- concentration and sodiation. SiO_2^- and PO_2^-, dominant in all profiles, also show a correlation with sodiation as differences in concentration can be seen. At sodiated regions, the SiO_2^- and PO_2^- profiles are much closer in concentration when compared to non-sodiated sites (Fig. 4a(i)).

The variation between SiO_2^- and PO_2^- profiles at the bulk region can be explained by differences in the regions chosen, rather than by sodiation as no distinct correlation can be seen as a function of current density. Therefore, it can be implied that the SEI formed is primarily composed of these oxide species and the change in concentration is driven electrochemically. These results support the *ex situ* literature data[8–11] suggesting that NASICON is not thermodynamically stable
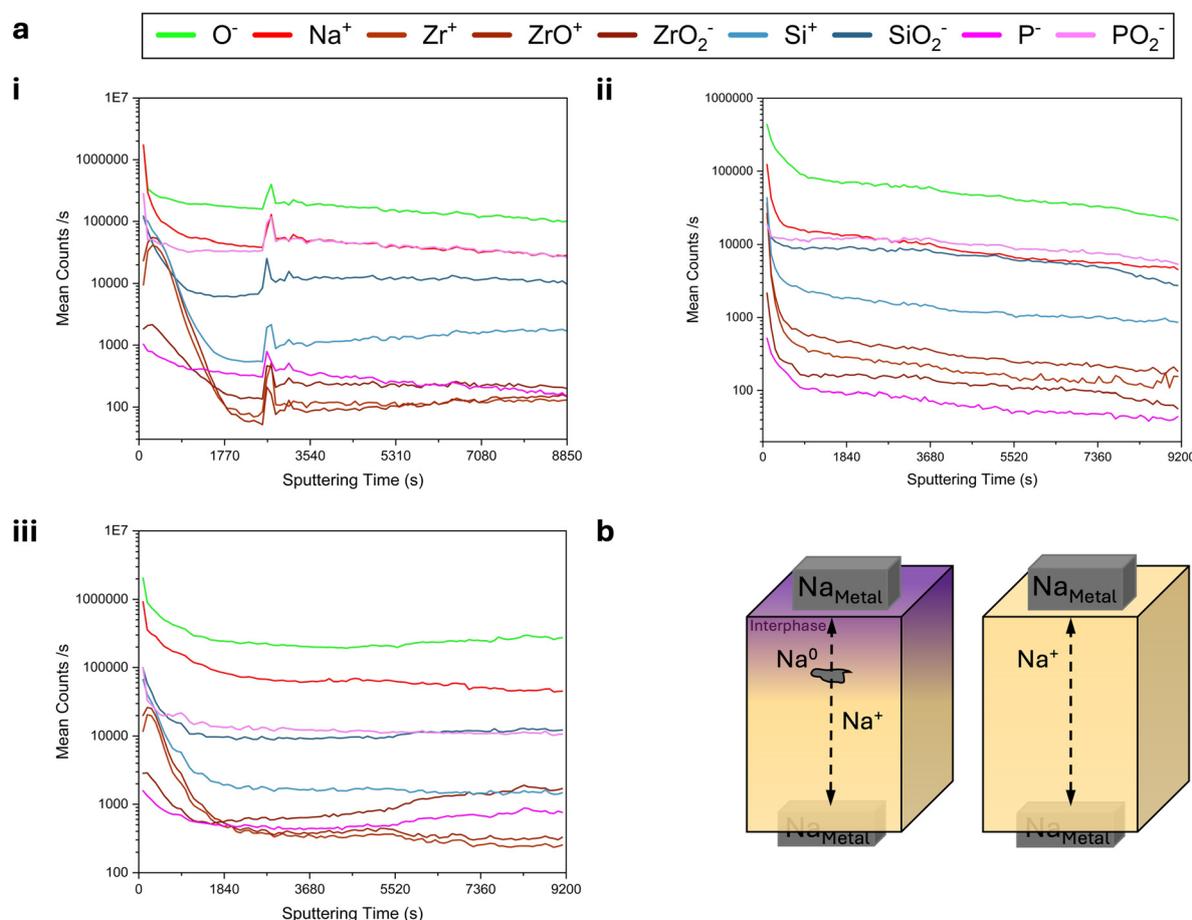
Fig. 4 Depth profiles of non-sodiated and sodiated regions. (a) Profiles of NASICON species and secondary phases with polarity chosen to maximise the yield. (i) A non-sodiated region, (ii) 0.04 μA μm⁻², and (iii) 0.1 μA μm⁻². (a)(i) Spike seen in the profile for the non-sodiated region is due to instrument artifact. (b) Schematic representation of the impact that the SEI has on sodium transport during cycling; dead sodium metal (Na⁰) nucleates inside the NASICON solid electrolyte due to reduced mobility along the grain boundaries.

against sodium and produces decomposition products including Na_2ZrO_3, Na_4SiO_4 and Na_3P that have sluggish Na^+ ionic conductivity.[18,19] The electrochemical change of the oxide species could be explained by the formation of these products, and contribute to the increase in concentration under sodiation. The SEI appears to propagate from the surface to the bulk region forming at grain boundaries, where sodium migration occurs, which degrades their functionality in sodium transport leading to dendrite formation (Fig. 4b).

Sodium transport columns and solid electrolyte interphase formation

To investigate the mechanism behind sodiation and correlation to SEI formation observed in the surface-to-bulk region, elemental ion maps were reconstructed in 3D. Reconstructions depicting sodiation and SEI formation are presented separately in Fig. 5 and 6 for a cycled and failed region, respectively. Reconstructions for other current densities can be found in Fig. S4–S7.† Differences in the yield and spatial locations of the Na^+ ions can be observed between non-sodiated, cycled and failed regions (Fig. 5). From Fig. 5(i), high concentration of Na^+ ions in the non-sodiated region is distributed across the surface to bulk region. In the cycled region (Fig. 5(ii)), concentrations and spatial locations of Na^+ ions have changed in the surface to near-surface region. It appears that a chemical layer is formed that is depleted of sodium, indicated by the decrease in counts and from the depth profile as shown in Fig. 4(ii), this layer can be identified as the SEI layer composed of the Zr, Si and P oxide species.

In comparison, Fig. 5(iii) shows high concentrations of Na^+ ions that extend from the surface towards the bulk of the NASICON. The concentrations appear as sporadic columns, and suggest that sodium metal has grown uncontrollably, forming metal filaments that have penetrated the NASICON. It can be inferred that the sporadic columns of Na^+ ions highlight the shape of the potential dendrite that has formed, as a result of applying a current density greater than the CCD. The 3D reconstruction suggests that through the bulk of the NASICON solid electrolyte, sodium creates transport columns directly under where the electric field is strongest (underside of the probe). These columns facilitate sodium mass transport, from the positive electrode towards the surface, and as sodium approaches the surface the electric field around the probe it becomes stronger, resulting in the nucleation of the sodium islands. As the applied current density increases, the electric field expands resulting in larger islands. This can be seen in Fig. S4(ii–iii),† where several columns are observed and verifies that along these transport columns dendrites may have formed. This has caused the sodium to form additional transport columns to allow mass transport towards the surface. For current densities below the CCD (Fig. S4(i)†), several observations can be made. A single mass transport column is present and towards the bulk, a reservoir of sodium is seen; this is formed due to the duration of the stripping process being less than that of plating (~30 min). It can be implied from this that the single column is not a dendrite, and facilitates sodium mass transport during cycling, and would explain the observed increase in the concentration of the ZrO_2^- profile in the bulk region (Fig. S3(i)†). To assess whether there is any correlation between sodiation and SEI formation, 3D reconstructions of the oxide species of interest in a non-sodiated region were used as a reference (Fig. 6(i)). In the non-
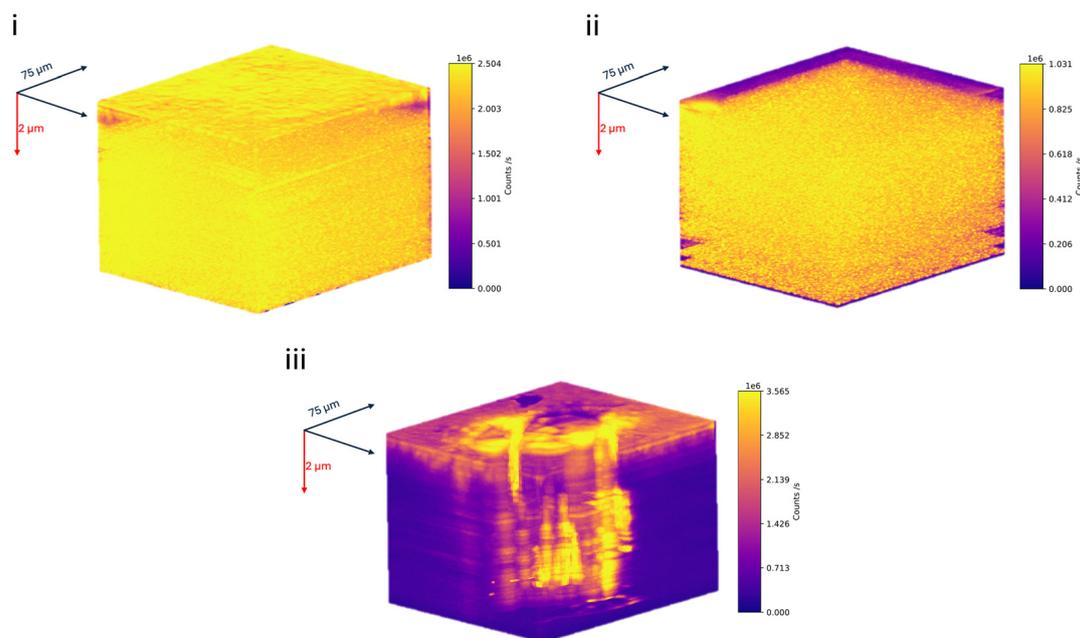
Fig. 5 3D reconstruction of Na^+ ion maps collected through dynamic SIMS in the sodiated region. (i) 3D reconstruction of the non-sodiated region, (ii) 0.04 μA μm^{-2}, and (iii) 0.1 μA μm^{-2}. Each 3D reconstruction represents the surface to bulk, and in (iii) areas of high concentrations of Na^+ ions represent transport columns. Colour bar has not been normalised and represents the inherent total counts collected for each region.
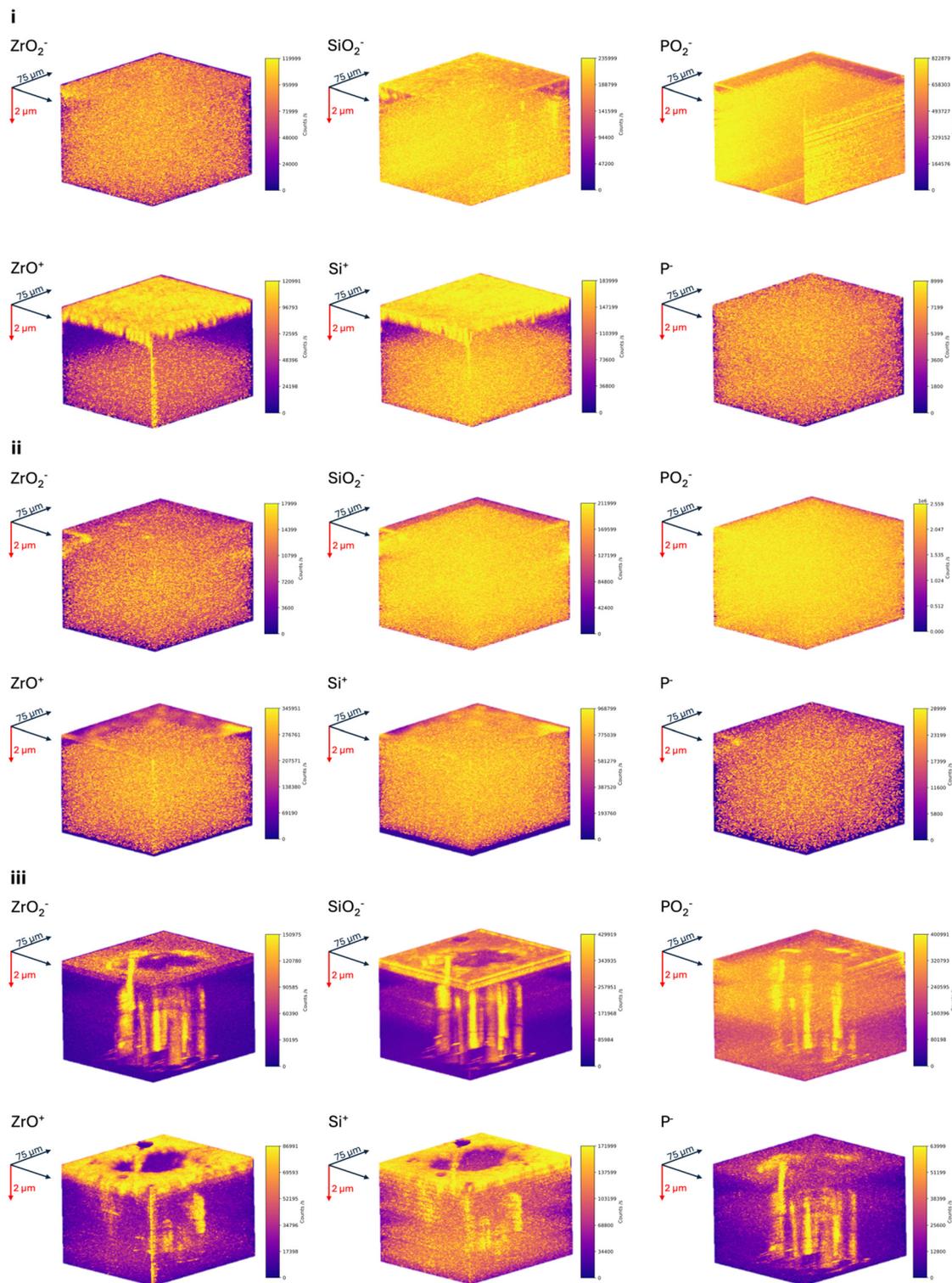
Fig. 6 3D reconstruction of oxide species correlated to SEI formation. (i) Non-sodiated region, (ii) 0.04 μA μm^{-2}, and (iii) 0.1 μA μm^{-2}. Columns represent the highest concentration of respective oxide species at each region. Colour bar has not been normalised and represents the inherent total counts collected for each region.

sodiated region, the surface-to-bulk region is mainly composed of SiO_2^- and PO_2^-, and the ZrO^+ and ZrO_2^- secondary phase(s) are located at the surface and surface-to-bulk region, respect-

ively. There is enrichment of Si^+ at the surface and near to the bulk, whereas the P^- is distributed across the surface to bulk region. In the cycled region (Fig. 6(ii)), changes in the second-

ary phase can be seen where ZrO^+ is now present in the surface-to-bulk region and hotspots of ZrO_2^- can be seen. Similarly, PO_2^- is present at the immediate surface and Si^+ and P^- species are distributed across the surface to bulk region. Reconstructions were also made for Zr^+, to assess whether similar observations could be made, and are presented for all current densities in Fig. S8.† From all data it can be suggested that through cycling the region has undergone a chemical change resulting in the formation of a SEI, that is indicated by the variations in spatial locations of oxide species.

In comparison, columns for all NASICON species can be seen in regions that have been partially stripped (Fig. S5†) and failed (Fig. 6(iii), Fig. S6 and S7†). The columns do not represent transport columns, as only sodium mass transport occurs, but instead serve to highlight the electrochemical reaction due to sodiation, validating that the SEI formation is driven kinetically and preferentially at the grain boundaries. Although the grain boundaries cannot be resolved in the 3D reconstructions, the preferential growth of the SEI along the grain boundaries was first indicated by the electrochemical degradation observed in the sodium transport mechanisms (Fig. 3 and Fig. S2†) and the change in the chemical composition of the sodium metal|NASICON interface by the formation of oxide species (Fig. 4 and Fig S3†). This is further supported by the dimensions and spatial locations of these columns, as they are small e.g. the smallest column observed in Fig. 6(iii) is ~6 μm wide, which would cover the grain boundaries residing in the NASICON as seen in Fig S10,† and are in the vicinity of the sodium transport columns, or in tandem for certain cases (Fig. S7†), highlighting the pathway of SEI formation through the bulk and grain boundaries of the NASICON during sodiation. However, there is some discrepancy and this is due to the transmission of Na^+ ions and beam conditions being optimised, to maximise the spatial resolution whilst mitigating beam dynamics influencing Na^+ ions to diffuse away from the surface.[13,20] Therefore, highly energetic Na^+ ions are not collected. This can be circumvented by tracking the O^- signal, presented for all current densities in Fig. S9.† The columns seen in the reconstructions are indicative of sodium transport columns, as not only do they match the locations of the transport columns but also indicate where the sodium has nucleated at the surface – due to the passivation reaction between sodium and NASICON. The reconstructions present the mechanism behind sodium mass transport and SEI formation, and more importantly, the SEI is not self-limited in contrast to previous literature reports.[8–10] The decomposition reaction products are a direct result of sodium transport, as sodium diffuses through the bulk and grain boundaries of the NASICON, the SEI forms along its pathway.

Conclusion

Through operando characterisation of a sodium-ion solid-state half-cell, regions of sodium metal|NASICON interfaces were formed and cycled at different current densities with the critical current density (CCD) found to be 0.04 μA μm^{-2} in a 1 μm^2 region. Cycled and failed regions were diagnosed to identify mechanisms behind sodiation and failure. It was found that as a function of current density, grain boundaries and an ion-conductive surface layer, formed due to sodiation, become increasingly resistive. Leveraging simultaneous dual-polarity dynamic SIMS, the surface layer was identified to be an SEI that is primarily composed of oxide species, ZrO_2^-, SiO_2^-, and PO_2^- and can be attributed to the decomposition products Na_2ZrO_3, Na_4SiO_4 and Na_3P that have sluggish ionic conductivity, as presented in the literature. Through 3D reconstructions, a mechanistic understanding of sodiation and SEI formation was obtained, and sodiation occurs through transport columns that extend from the positive electrode to where the load is established. Along these transport columns and around, decomposition products form an SEI that is not self-limited. The SEI forms along the pathway of sodiation, bulk and grain boundaries, impeding sodium migration, and at current densities higher than the CCD a dendrite is formed. This work has presented a new key insight into the mass transport and failure mechanism in a solid-state sodium-ion battery. The technique also serves as a diagnostic tool to develop engineering solutions for interfaces and solid electrolytes that can be applied to other systems such as lithium-ion batteries and supercapacitors to pave the way for next-generation energy-storage devices.

Methods

Materials

$Na_{3.4}Zr_2Si_{2.4}P_{0.6}O_{12}$ (NZSP) was synthesised via solution-assisted solid-state synthesis developed as previously reported.[19] Precursors, including $NaNO_3$ (99%), $ZrO(NO_3)_2$ (99%), $Si(OC_2H_5)_5$ (99%) and $NH_4H_2PO_4$ (99.5%), were sourced from Sigma Aldrich. Pellet samples were uniaxially pressed using a 10 mm diameter die under a load of 1.5 tonnes and then sintered in a Pt crucible at 1285 °C for 5 hours at a heating and cooling rate of 300 °C h^{-1}.

Preparation of samples

One side of the sintered NZSP pellet was ground using SiC pads (Struers, grit sizes: 1200, 2000, and 4000) with ethanol (VWR ethanol absolute >99.8%) acting as a lubricating solvent. Pellet samples were then sonicated in ethanol for 15 minutes before polishing the ground surface using alcohol-based diamond suspension (Struers, suspension sizes: 3 μm, 1 μm and μm).

Solid-state half-cell setup

Polished NZSP was then placed into an argon-filled glovebox (MBraun O_2 < 2 ppm and H_2O < 0.3 ppm) directly after preparation. The sodium metal electrode (99.9%, Sigma Aldrich) was punched using a 3 mm diameter die and mechanically stacked onto the unpolished side of NZSP using a glass gasket.

The sodium electrode was encased using indium (diameter of 8 mm) to act as a protective barrier and current collector. The prepared NZSP pellet was then placed on top of a glass substrate (diameter of 5 mm), which insulates the half-cell from the instrument, and fixed in a position using a copper clip on the Hi-5 sample mount holder.

Characterisation

Operando characterisation was carried out using the Hi-5 SIMS instrument (Hiden Analytical, United Kingdom). The primary ion gun used was 2 keV Xe^+ and a Biologic SP-240 potentiostat, with Kleindiek probes (tip area of 1 μm^2), was used for electrochemical measurements. Constant currents of 0.02 μA ($J = 0.02\ \mu A\ \mu m^{-2}$), 0.04 μA ($J = 0.04\ \mu A\ \mu m^{-2}$), 0.06 μA ($J = 0.06\ \mu A\ \mu m^{-2}$), 0.1 μA ($J = 0.1\ \mu A\ \mu m^{-2}$), 0.2 μA ($J = 0.2\ \mu A\ \mu m^{-2}$) and 0.5 μA ($J = 0.5\ \mu A\ \mu m^{-2}$) were repeatedly applied at different regions across the NZSP polished surface to generate sodium islands. Cycle graphs were recorded for each current measurement with a time step of 5 s. Electrochemical Impedance Spectroscopy (EIS) data were collected using a perturbation voltage of 300 mV to reduce noise in the frequency range of 7 MHz to 100 Hz. Voltage safety limits for all electrochemical measurements were set to ±10 V and simultaneous positive and negative polarity were used for all SIMS measurements. Cycle graphs and EIS spectra were recorded using EC-Lab (BioLogic, France). EIS spectra were analysed using RelaxIS 3 (rhd instruments, Germany). Depth profiles were recorded and analysed using a Hiden SIMS mapper (Hiden Analytical, United Kingdom) and 3D plots were constructed using in-house software written in Python 3.9. SEM images were obtained using Hi5-SIMS and Zeiss Auriga microscope instruments. For the Hi5-SIMS instrument, a working distance of 14 mm and a beam accelerating voltage of 2 keV were used. For the Zeiss Auriga microscope, an in-lens detector, a working distance of 6 mm, a beam accelerating voltage of 10 kV, and a 30 μm aperture were used.

Author contributions

S. S. conceived, designed and conducted the experiment, analysed the data and wrote the in-house software for 3D analyses, and developed the *operando* technique. R. J. C., S. F., G. C. and N. S. assisted with the calibration of the instrument to undertake this work, and S. J. S. provided supervision. All authors reviewed and discussed the results and analyses for the final manuscript.

Conflicts of interest

The authors declare no conflicts of interest.

Data availability

The research data that support this article are available on Zenodo (**https://zenodo.org/communities/electroceramic-materials**).

Acknowledgements

References

1 J.-S. Hwang, S.-T. Myung and Y.-K. Sun, Sodium-ion batteries: present and future, *Chem. Soc. Rev.*, 2017, **46**, 3529–3614.

2 T. Liu, Y. Zhang, Z. Jiang, X. Zeng, J. Ji, Z. Li, X. Gao, M. Sun, Z. Lin, M. Ling, J. Zheng and C. Liang, Exploring competitive features of stationary sodium ion batteries for electrochemical energy storage, *Energy Environ. Sci.*, 2019, **12**, 1512–1533.

3 M. D. Slater, D. Kim, E. Lee and C. S. Johnson, Sodium-Ion Batteries, *Adv. Funct. Mater.*, 2013, **23**, 947–958.

4 H. Y.-P. Hong, Crystal structures and crystal chemistry in the system $Na_{1+x}\ Zr_2\ Si_x\ P_{3-x}\ O_{12}$, *Mater. Res. Bull.*, 1976, **11**, 173–182.

5 J. B. Goodenough, H. Y.-P. Hong and J. A. Kafalas, Fast Na^+-ion transport in skeleton structures, *Mater. Res. Bull.*, 1976, **11**, 203–220.

6 C. Yang, S. Xin, L. Mai and Y. You, Materials Design for High-Safety Sodium-Ion Battery, *Adv. Energy Mater.*, 2021, **11**, 2000974.

7 L. Ran, A. Baktash, M. Li, Y. Yin, B. Demir, B. Lin, M. Li, M. Rana, I. Gentle, L. Wang, D. J. Searles and R. Knibbe, Sc, Ge co-doping NASICON boosts solid-state sodium ion batteries' performance, *Energy Storage Mater.*, 2021, **40**, 282–291.

8 C. Li, R. Li, K. Liu, R. Si, Z. Zhang and Y.-S. Hu, NaSICON: a promising solid electrolyte for solid-state sodium batteries, *Interdiscip. Mater.*, 2022, **1**, 396–416.

9 Z. Zhang, S. Wenzel, Y. Zhu, J. Sann, L. Shen, J. Yang, X. Yao, Y.-S. Hu, C. Wolverton, H. Li, L. Chen and J. Janek, $Na_3Zr_2Si_2PO_{12}$: A Stable Na^+-Ion Solid Electrolyte for Solid-State Batteries, *ACS Appl. Energy Mater.*, 2020, **3**, 7427–7437.

10 T. Ortmann, S. Burkhardt, J. K. Eckhardt, T. Fuchs, Z. Ding, J. Sann, M. Rohnke, Q. Ma, F. Tietz, D. Fattakhova-Rohlfing, C. Kübel, O. Guillon, C. Heiliger and J. Janek, Kinetics and Pore Formation of the Sodium Metal Anode on NASICON-Type $Na_{3.4}Zr_2Si_{2.4}P_{0.6}O_{12}$ for Sodium Solid-State Batteries, *Adv. Energy Mater.*, 2023, **13**, 2202712.

11 Z. Gao, J. Yang, H. Yuan, H. Fu, Y. Li, Y. Li, T. Ferber, C. Guhl, H. Sun, W. Jaegermann, R. Hausbrand and Y. Huang, Stabilizing $Na_3Zr_2Si_2PO_{12}$/Na Interfacial Performance by Introducing a Clean and Na-Deficient Surface, *Chem. Mater.*, 2020, **32**, 3970–3979.

12 E. Quérel, N. J. Williams, I. D. Seymour, S. J. Skinner and A. Aguadero, Operando characterization and theoretical

modeling of metal|electrolyte interphase growth kinetics in solid-state batteries. part i: Experiments, *Chem. Mater.*, 2023, **35**, 853–862.

13 S. Sukumaran, S. Fearn and S. J. Skinner, In situ TOF-SIMS investigation of the dynamic metallic anode|solid electrolyte interface in solid-state sodium-ion batteries, *Cell Rep. Phys. Sci.*, 2025, **6**, 102447.

14 R. J. Chater, A. J. Smith and G. Cooke, Simultaneous detection of positive and negative secondary ions, *J. Vac. Sci. Technol., B:Nanotechnol. Microelectron.:Mater., Process., Meas., Phenom.*, 2016, **34**, 03H122.

15 H. Gao, S. Xin, L. Xue and J. B. Goodenough, Stabilizing a High-Energy-Density Rechargeable Sodium Battery with a Solid Electrolyte, *Chem*, 2018, **4**, 833–844.

16 Q. Ma, C.-L. Tsai, X.-K. Wei, M. Heggen, F. Tietz and J. T. S. Irvine, Room temperature demonstration of a sodium superionic conductor with grain conductivity in excess of 0.01 S cm^{-1} and its primary applications in symmetric battery cells, *J. Mater. Chem. A*, 2019, **7**, 7766–7776.

17 J. T. S. Irvine, D. C. Sinclair and A. R. West, Electroceramics: Characterization by Impedance Spectroscopy, *Adv. Mater.*, 1990, **2**, 132–138.

18 V. Lacivita, Y. Wang, S. H. Bo and G. Ceder, Ab initio investigation of the stability of electrolyte/electrode interfaces in all-solid-state Na batteries, *J. Mater. Chem. A*, 2019, **7**, 8144–8155.

19 S. Umesh, V. K. Jayaraman, V. Dhanasekaran and S. P. Annigere, Enhanced sodium ion conduction in Al-substituted Na_2ZrO_3, *Mater. Lett.*, 2021, **304**, 130713.

20 M. Collin, S. Gin, P. Jollivet, L. Dupuy, V. Dauvois and L. Duffours, ToF-SIMS depth profiling of altered glass, *npj Mater. Degrad.*, 2019, **3**, 14.